GEOPHYSICS, VOL. 58, NO. 1 (JANUARY 1993); P. 121-133, 10 FIGS.

3-D physical modeling and pseudospectral simulation of seismic common-source data volumes

How-Wei Chen* and George A. McMechan*

ABSTRACT

Numerical simulation of common-source seismic responses of arbitrarily complicated three-dimensional (3-D) variable-velocity structures is implemented by pseudospectral solution of the scalar wave equation. Potential applicability of such simulation to data analysis and interpretation is demonstrated by comparing synthetic 3-D *(x, y, t)* common-source gathers with those recorded on an area1 grid of receivers over a physical scale model of a salt tongue. The iterative model adjustment process in fitting the physical model data is analogous to that which would be required for field data. Comparing differences between 2-D and 3-D synthetic responses allows interpretation of out-of-plane propagation. It is necessary to include the effects on the source directivity, because of a shield placed over the source during data acquisition, to numerically approximate the main features in the recorded scale model data.

INTRODUCTION

Through the increasing availability of large-scale computing resources, prestack three-dimensional (3-D) seismic modeling and migration are now feasible. Prestack common-source modeling algorithms for 3-D scalar and elastic wave equations include finite-differences (Mufti and Fou, 1989; Chang and McMechan, 1989; Mufti, 1989, 1990; Yoon and McMechan, 1991) and the pseudospectral method (Reshef et al., 1988a and b). Even algorithms for prestack modeling in anisotropic media have been developed (Mora, 1989; Dong and McMechan, 1991). Prestack migration for 3-D shot gathers has been implemented for both isotropic and anisotropic media (Chang and McMechan, 1990; Dong and McMechan, 1993; Reshef, 1991).

Mufti (1989, 1990) and Mufti and Fou (1989) present synthetic examples that demonstrate the desirability and utility of simulating seismic data for realistically complicated 3-D structure models for analysis and interpretation. Our goal in the present paper is to go beyond the synthetic examples used in those papers to direct application to, and analysis of, scale model data.

Scale model data have many advantages for testing purposes; the model and acquisition geometry are controlled and the data have many of the characteristics of field data (noise, source directivity, full 3-D responses). Thus, experiment designs and data processing may be evaluated using scale model data without the cost of field acquisition (e.g., Ladzekpo et al., 1988; Lu and Herbert, 1989; Ebrom et al., 1990). We explicitly illustrate the ability to simulate the main features in the recorded data; differences between 2-D and 3-D responses; and strong effects, on source directivity, on placing a shield around part of the source. The difficulties in estimating internal velocities and geometries were addressed by consideration of the effects of systematic, iterative mode adjustments across the data for all sources; a similar procedure would be required for fitting field data.

3-D PSEUDOSPECTRAL MODELING

The physical model data that follow were acquired in water tank, so we use the scalar wave equation for numeric; simulations. Assuming constant density, this equation is

$$\frac{\partial^2 P}{\partial x^2} + \frac{\partial^2 P}{\partial y^2} + \frac{\partial^2 P}{\partial z^2} = \frac{1}{C^2(x, y, z)} \frac{\partial^2 P}{\partial t^2} - S(x, y, z, t), \qquad (1)$$

where P is acoustic pressure; x, y , and z are Cartesia spatial coordinates; t is time; S is the source; and C is the local velocity. Equation (1) is solved by the pseudospectra method described by Reshef et al. (1988a), in which the partial derivatives in space are computed by multiplicatic by wavenumber in the Fourier domain and the parti derivatives in time are computed by second-order fini differencing in the time domain. The characteristics of pse dospectral algorithms are described in Kreiss and Olig (1972), Gazdag (1973), Orzag (1981) and Holberg (1987).

Manuscript received by the Editor October 4, 1991; revised manuscript received June 25, 1992.
*Center for Lithospheric Studies, The University of Texas at Dallas, P. O. Box 830688, Richardson, TX 75083-0688.

Their main advantages are that they are numerically very stable, and for a given accuracy, require fewer grid points per wavelength than traditional finite differencing (Kosloff and Baysal, 1982; Fornberg, 1987; Daudt et al.. 1989).

Absorbing boundaries are applied using the amplitude tapering approach in Cerjan et al. (1985). At the top surface of the model volume, either the absorbing or the free-surface ($P = 0$) condition may be selected. Both sources and receivers in the physical model are well below the water surface; thus, free-surface multiples could be ignored and, for the following calculations, the top of the model has been specified to be absorbing.

The point source

$$S(x, y, z, t) = \delta(x - x_0)\delta(y - y_0)\delta(z - z_0) \times \exp[-\pi (I - t_0)^2] \quad (2)$$

may be located anywhere in the grid at (x_0, y_0, z_0). t is the time since the source excitation and t_0 is the time shift required to make the wavelet causal. For many of the computations below. the source directivity is modified by simulation of a shield that covers the top, back, and one side of the source.

Implementation is in a CRAY-YMP and uses the multiple-vector mixed-radix Fourier transform CFFTMLT from the CRAY Unicos Math and Scientific Library. Each time step involves one forward and one inverse 3-D Fourier transform. For the 180 x 180 x 90 grid used in the computations below, each time step (including output to disk) took 3.03 s. Since this is a numerical grid method, the computational cost is independent of the complexity of the model and responses are available at all grid points at all time steps.

PHYSICAL MODEL DATA ACQUISITION

In the spring of 1990. ten 3-D common-source gathers were collected over a scale model of a salt tongue embedded in a sequence of horizontal layers at the Seismic Acoustics Lab (SAL) at the University of Houston. The model (designated #57 in the SAL catalog) was designed and sculpted by Walt Turpening of BP Exploration. This model has been used in a number of previous studies (Ladzekpo et al., 1988; Lu and Herbert, 1989: Chon and Turpening, 1990). The present study is the first to synthesize 3-D common-source data recorded on a complete (x, y) grid rather than on selected lines, for any physical model.

For recording, the model was submerged in a water tank. For each of ten source locations (Figure I) the acoustic pressure response was recorded on a 240 x 240 regular grid of receiver locations. Figure 1 shows a view looking down on the top of the tank, including the model and surrounding water, the source and receiver positions, the locations of the slices in Figure 2, and contours on the embedded salt body. The recording grid is shifted relative to the model in an attempt to capture reflections from the steeply dipping front of the salt.

Figure 2 shows five vertical, constant-x and five vertical, constant-y slices through the numerical model that approximates the submerged physical model. The actual dimensions of the model are (x, y, z) = (0.61, 0.61, 0.24) m. After enlarging the volume considered to include the surrounding water, and the space for application of the absorbing boundary conditions (15 grid points on all edges) during the numerical computations. and scaling of the model up to real-world dimensions, the computational volume has dimensions (x, y, z) = (21.96, 21.96, 10.92) km. Scaled *P-wave* velocities are shown in Figure 2. The source transducer was a Celesco LC-IO; the receiver transducer, a Celesco LC-5. These transducers have nearly flat spectra from 5 kHz to 200 kHz: after filtering and scaling, the physical model seismograms have signal frequencies between 5 and 18 Hz and a dominant frequency of approximately 10 Hz. Background noise of higher frequencies is also present. The synthetics have a similar bandwidth, with a dominant frequency of approximately 12 Hz. The scaled dimensions of the transducers are very large ($\approx 10^2$ m) compared to sources and receivers in real surveys.

One of the unusual features of the survey configuration was that a polystyrene shield was attached to the source transducer in an attempt to reduce ringing in the source signature, and to direct the energy in a predominantly downward direction (K. K. Sekharan, personal communication). The directivity produced by this shield had a strong asymmetrical effect on the energy distribution in the data; simulating this was a major task in the numerical modeling. A source shield would be partly reflecting, partly absorbing, and partly transmitting of the source energy. These physical characteristics are not possible to simulate numerically with the small number of grid points available. For expediency, we simulated a completely reflecting shield (implemented on a surface of one grid point thickness, by setting the propagating field $P = 0$). In view of the results, this approximation appears reasonable.

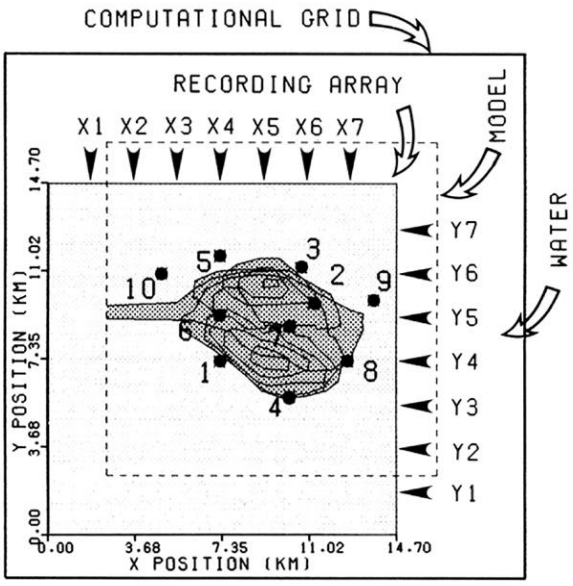

FIG. 1. Experiment geometry; top view. Numbered points are source locations. Labeled arrows show locations of the cross-sections in Figure 2. Contours are on the surface of the salt tongue. The shaded rectangle is that covered by the receiver grid. Dimensions are scaled up to "real world" size.

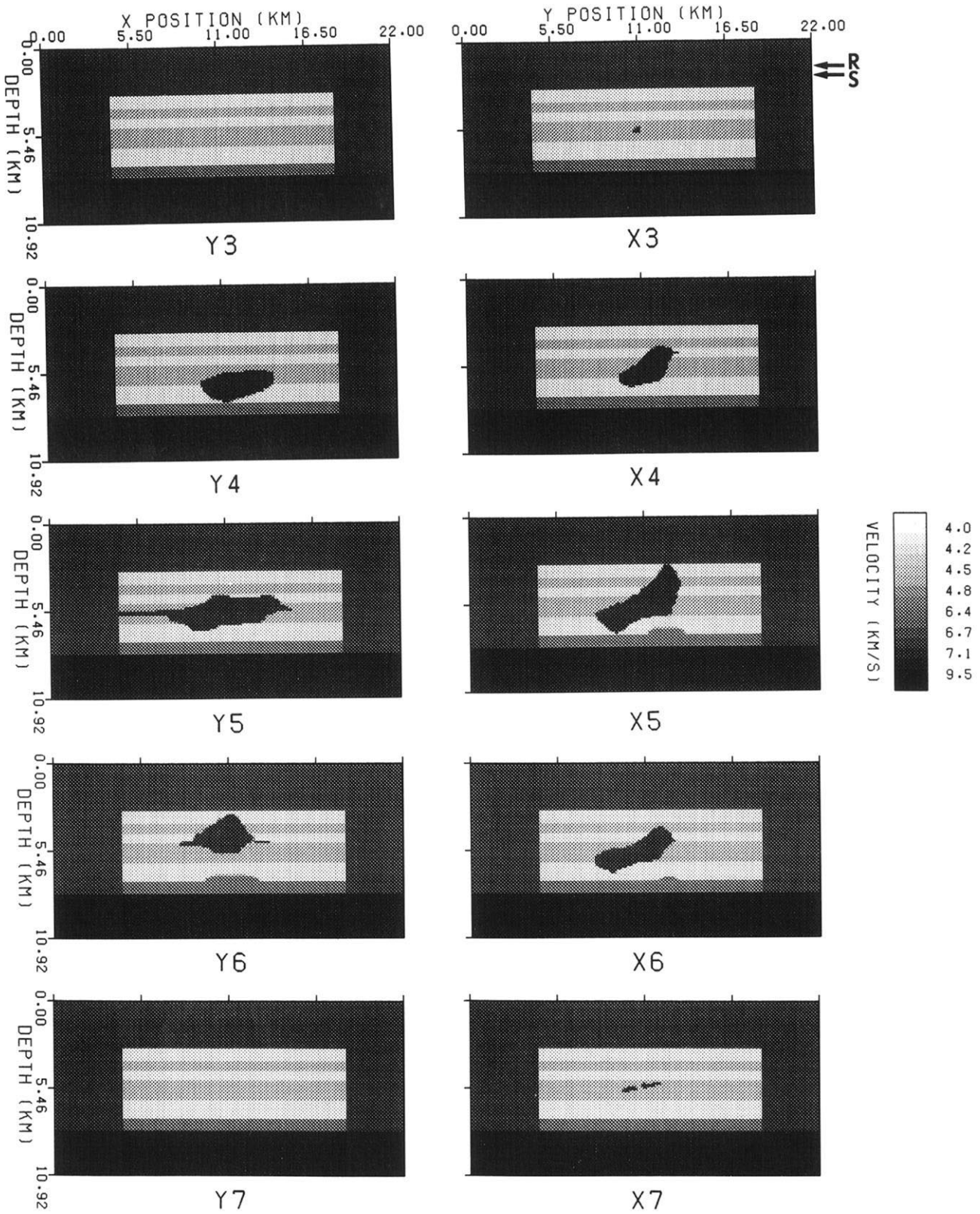

FIG. 2. Model cross-sections. Slice locations are identified in Figure 1. Arrows S and R show the source and receiver depths, respectively. The gray scale gives *P*-wave velocities.

MODELING RESULTS

In this section, we first demonstrate the viability of 3-D modeling for interpretation of 3-D common-source data by direct comparison of synthetic and physical model data. Then, we illustrate the importance of the effects of source directivity and 3-D propagation in the physical model data. The former is achieved by numerical simulation of a shield over part of the source; the latter, by comparing 2-D and 3-D synthetics with each other and with the corresponding physical model data.

Comparison of physical model and numerical results

Figure 3 shows four representative vertical, fixed-y slices through the 3-D (x, y, t) data volume for source 1 recorded in the model tank (above) and the corresponding synthetic output (below). Figure 4 shows four vertical, fixed-x slices from the same tank and synthetic data volumes in the same format. Although the recorded and synthetic data differ in specific details, the general characteristics, and the changes from slice to slice, are similar in the tank and synthetic data. In these, and all subsequent plots, a single, but different, scale factor is applied to each synthetic and model tank data volume; the relative scaling was chosen to give approximately the same average amplitude for each volume.

A comparison of the data and the corresponding model for any given line position shows that the salt produces a shadow zone for reflections lying beneath it; this shadow is the result of a combination of geometrical scattering and masking by the highly reflective salt. Specific arrivals are identified in the figure captions.

To obtain the correspondence between the observed and calculated data in Figures 3 and 4, it was necessary to have accurate scaling of the tank data; a good numerical representation of the complicated 3-D salt tongue; information on the positions of the sources and recording array relative to each other, to the external edges of the model, and to the interfaces and salt tongue within the model; and the source directivity. The least well-known factor at the start of the study was the source directivity. Although nominal values were available for all these inputs, the associated uncertainties were sufficient that better results could be achieved by iterative perturbations of the velocities, and of the geometries of the salt and the source and of the source shield. The numerical results shown here and for other sources (below) occur after about 30 iterations, and in each of them, recorded and synthetic data from a number of source positions were compared simultaneously to constrain model and source adjustments. The residual differences in the final plots are now believed to be primarily related to inaccuracies in the specification of the shape and the (necessarily) discrete form of the salt tongue in the numerical model. Similar limitations would be present in simulation of field data.

Since both the scale model and synthetic common-source data are (x, y, t) volumes, any desired data partitions may be displayed. For example, consider data recorded on a single slice through the center of the data volumes, for a number of sources. Figure 5 contains the observed and synthetic data on line Y4 (Figure 1) from sources 5,6,7, and 9. As in Figures 3 and 4, the synthetics are able to predict the main features in the observations.

Effects of source directivity

In computing the synthetic seismograms in Figures 3 to 5, a strong source directivity was included. Although some effects of this directivity are visible, for example, in the right-to-left asymmetry in the first-break amplitudes and wavelet shapes, and the pronounced energy decrease E in Figure 4, the overall importance of source directivity cannot be ascertained from the final figures alone. To illustrate, we shall now compare open point source and shielded point source synthetics with selected representative data slices.

The polystyrene shield that was taped to the source transducer during acquisition produced a strong (unintended) directivity in addition to the intended damping of source ringing. The exact shape and dimensions of this shield are not known, so they were approximated empirically by iterative modeling. The level of detail and smoothness of the simulated shield were restricted by the grid increment; the final best-fit geometry obtained is displayed in Figure 6. This shield significantly reduces the amount of energy propagating in the $+y$ and $+x$ directions, and, increases it in the $-y$ and $-x$ directions. Interference between the direct wave from the source and energy reflected inside the shield further complicates the directivity of the resulting apparent source.

Figures 7 and 8 provide a comparison of observed and synthetic data for source 1 on the two orthogonal slices X4 and Y4. Synthetic data were computed both without, and with, the source-shield, in 2-D and 3-D. A comparison of the 3-D responses with and without the shield in Figure 7 shows strong damping of energy to the right (large X) of the source produced by the vertical panel C on the shield (Figure 6); Figure 8 shows that this effect is confined to a narrow zone in y. Comparing the 3-D responses with and without the shield in Figure 8 shows that panels A and B (Figure 6) have a broad influence in decreasing amplitude to the right (large Y) of the source. Figures 9 and 10 show similar behavior in data for sources 6 and 7. The shield also produces the decrease in amplitude from left-to-right in the panels of Figure 4.

Comparison of 2-D and 3-D responses

The synthetic responses considered previously have all been fully 3-D, so the source directivity and geometrical spreading effects have been 3-D. In this section, we compare 2-D and 3-D responses, as an aid to identification of out-of-plane propagation. In doing this, new source directivity effects are necessarily introduced because 2-D calculations imply line rather than point sources. The spreading of a cylindrical wave from a line source corresponds to an $r^{-1/2}$ amplitude decrease, compared to r^{-1} for a spherical wave from a point source; thus the relative amplitudes of deep reflections tend to be too large in 2-D calculations.

Figures 7 and 8 show 2-D and 3-D synthetic responses on slices Y4 and X4 for source 1 with and without the source shield. These slices were chosen because they go approximately through their respective source locations. Similarly, Figures 9 and 10 contain slices Y5 for source 6 and X6 for source 7.

In Figures 7 and 8, offline reflections A and B from the vertical model edges are present only in the 3-D responses. The shield strongly influences both 2-D and 3-D responses,

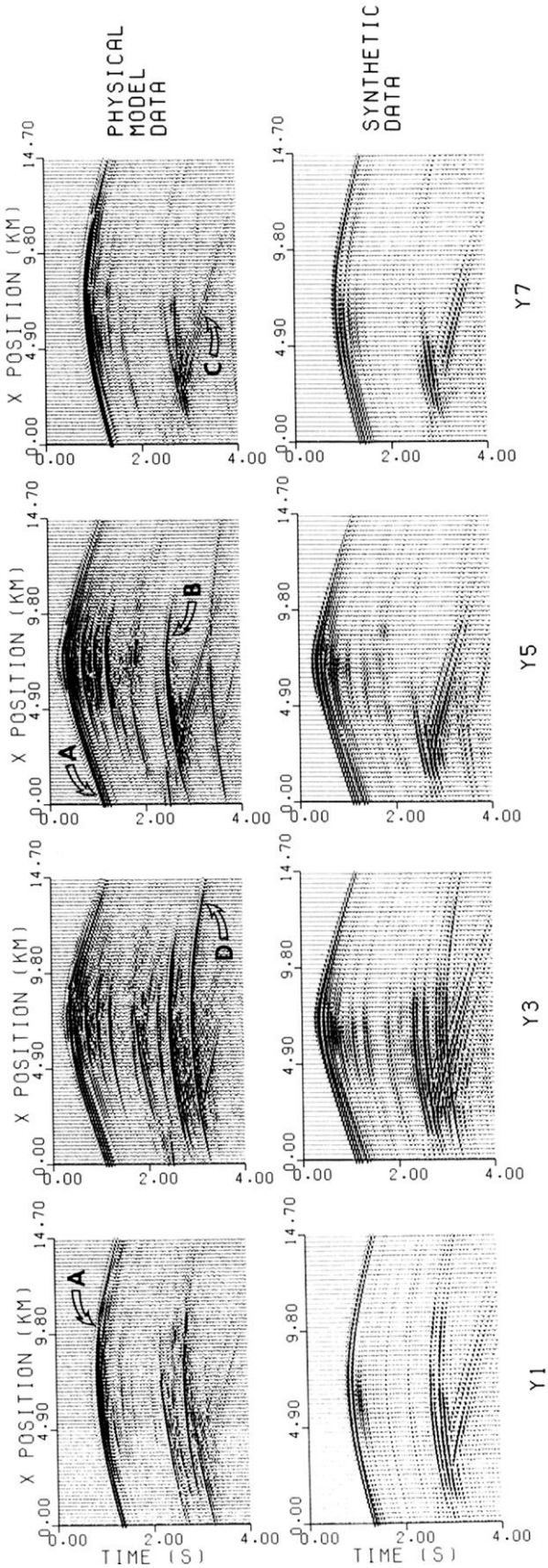

FIG. 3. Physical model data (top) and synthetic data (bottom). These data are for source 1. The locations of these constant-y recorder lines are shown in Figure 1. True relative amplitudes are used, both within and between plots. A is the direct arrival, B is a reflection from the bottom of the model, C is a reflection from the vertical edge at x = 2.5 km, D is a reflection from the vertical edge at y = 2.5 km, and reflections between A and B are from the horizontal reflectors and the salt tongue. Data slices orthogonal to these are shown in Figure 4.

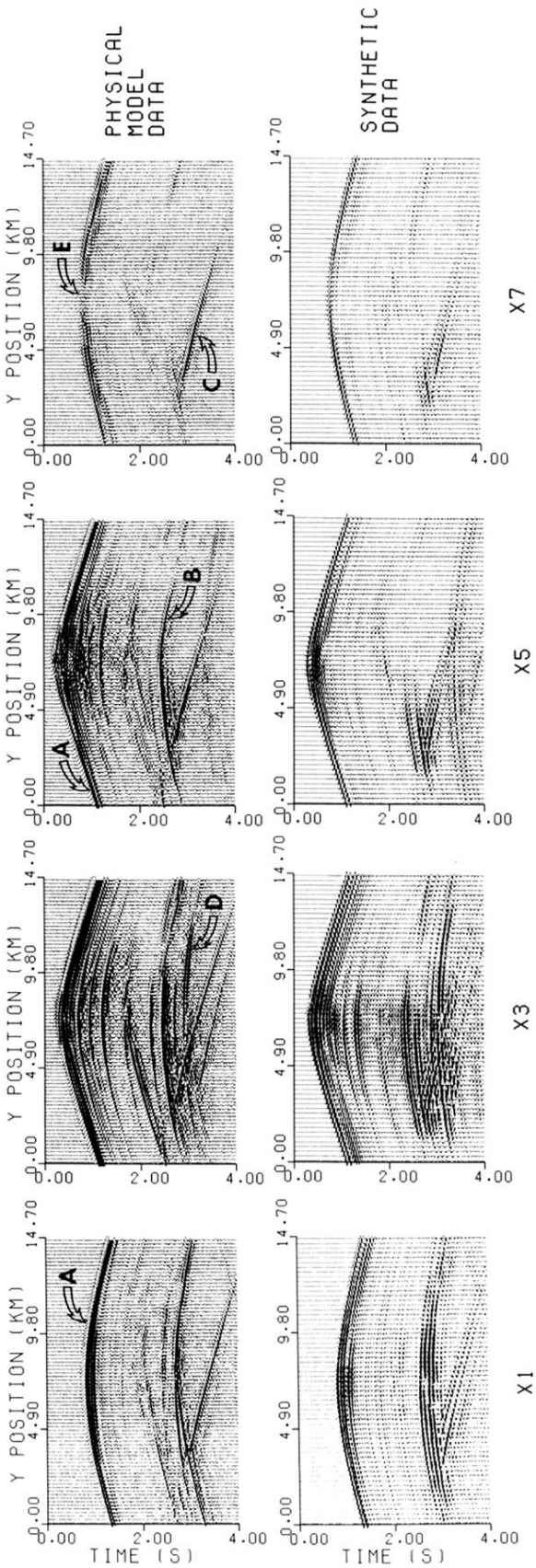

FIG. 4. Physical model data (top) and synthetic data (bottom). These data are for source 1. The locations of these constant-x recorder lines are shown in Figure 1. True relative amplitudes are used, both within and between plots. A is the direct arrival, B is a reflection from the bottom of the model, C is a reflection from the vertical edge at y = 2.5 km, D is a reflection from the vertical edge at x = 2.5 km, and reflections between A and B are from the horizontal reflections and the salt tongue. The energy decrease at E in the first break is due to the source directivity. Data slices orthogonal to these are shown in Figure 3.

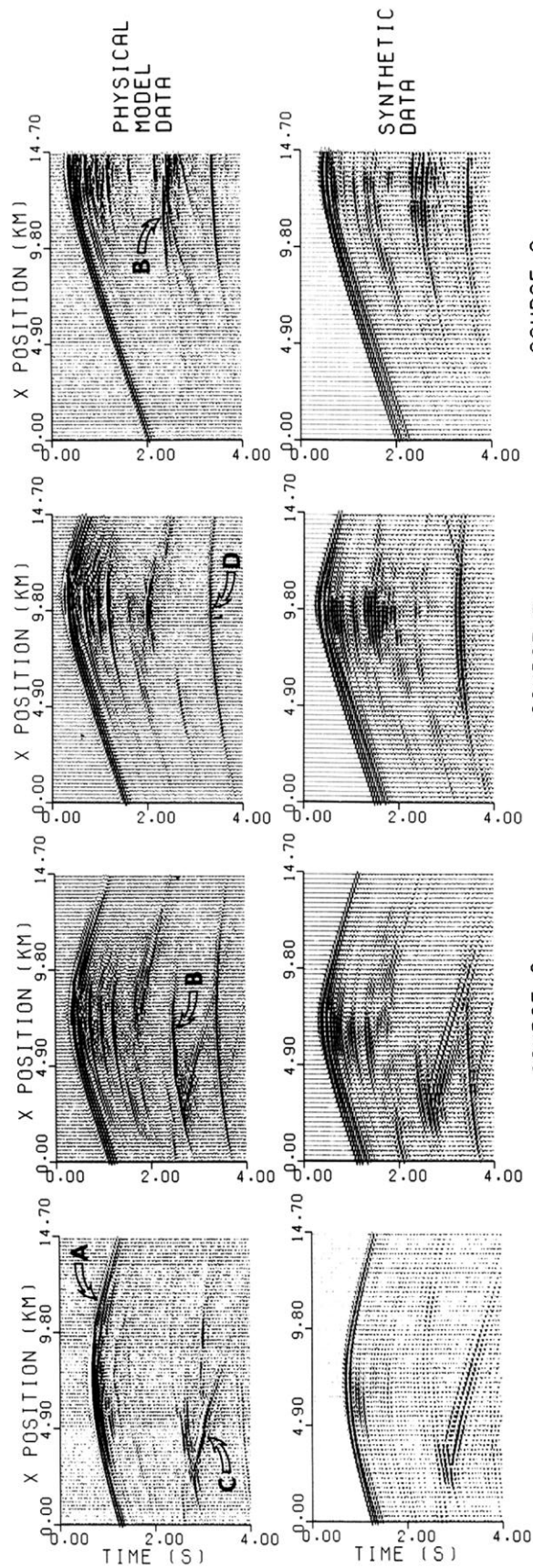

FIG. 5. Physical model (top) and synthetic (bottom) data for four sources on constant-x receiver slice Y4 (Figure 1). Labeled arrivals correspond to those similarly labeled in Figure 3.

making some less visible (see B in Figure 7) and others more visible (see C in Figure 7), depending on the net masking. energy beaming, and interference patterns.

In the line Y5 data from source 6 in Figure 9, the strongly focused energy A that is reflected from the Salt off-line is reproduced only by the synthetic 3-D response with the shield. Also, the off-line edge reflection B is only reproduced by the 3-D calculations. The high relative amplitudes of reflections from the model bottom and edge (C) in the 2-D calculations are associated with 2-D cylindrical spreading. Energy D. reflected from the top of the salt in the 2-D. unshielded-source data, moves offline and is not visible in the corresponding 3-D data. and is further suppressed by the shield. The same general behaviors are seen in the line X6 data from source 7 in Figure IO.

DISCUSSION AND SYNOPSIS

The major features in the observations have been consistently well predicted throughout (x, y, t) data volumes for a variety of source positions for a single 3-D model. The remaining discrepancies may be attributed to differences between details of the shape of the physical and numerical salt tongue models and source shield, effects of discretization of the numerical model, spectral differences, uncertainties in source and receiver positions in the model, and the fact that the shape and position of the source shield may have been changed during the survey, which took about two weeks to complete.

As may be expected, the accuracy of modeling is inversely proportional to the complexity of the feature involved. Strong reflections from the planar model bottom and vertical edges were best reproduced, followed by those from the internal horizontal interfaces, followed by those from the complicated 3-D salt tongue. The fit of the latter could certainly be improved by using a finer computational grid and doing additional iterative adjustments of position and shape. Identification of 3-D effects is facilitated by comparing 2-D with 3-D responses for a number of data slices.

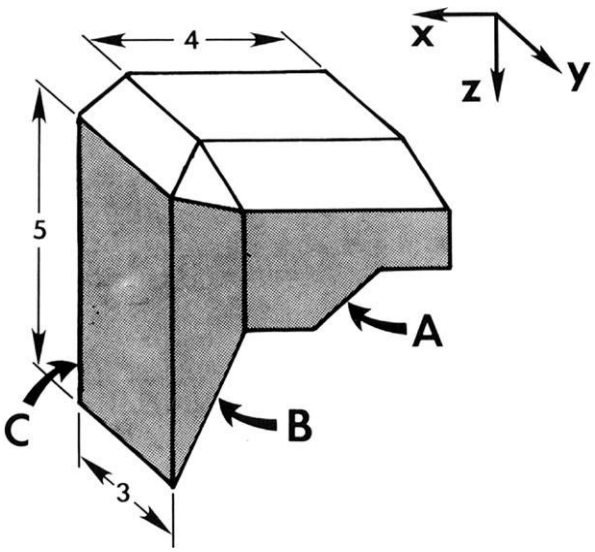

FIG. 6. The source-shield model. Dimensions are in units of grid points. This is a view of the back of the shield, to show the shape of the vertical sides. Segments A, B, and Care not present at the edges that are hidden in this view. The point source location is inside, near the center of the upper plane, at the depth where the sloping and vertical edges meet.

One assumption in this study is that the scalar wave equation [equation (1)] provides an adequate approximation of wave propagation in the model tank; the effects ofchanges in density upon reflectivity. and converted shear waves have been neglected. In view of the materials used in the model, and the nearly linear relation between density and P-wave velocity (e.g., Gregory. 1977), such effects are not expected to alter our main observations or conclusions. More complete, more accurate 3-D synthetic responses could have been produced, for example by the 3-D. variable density. elastic, staggered grid formulation of Yoon and McMechan (1991), but the associated additional expense does not appear to be justified in this case.

While the scale model data do have many of the characteristics of field data, they also have their own limitations. The defects of model data. are. for the most part, not present in actual seismic data and, therefore, are not an advantage of physical scale modeling. For example, ultrasonic transducers are naturally resonant and narrow-band due to physical properties which are totally unlike vibrators or explosive seismic sources. Ultrasonic transducers are also usually one or several wavelengths in size: this products directivity completely unlike those encountered in field conditions. The numerical and tank data are different in many ways, and that difference is very instructive about the limitations of both modeling techniques.

Both data acquisition and numerical modeling provided (x. y, t) data volumes. Only selected slices from these volumes were presented here to facilitate the discussion. The data volumes are amendable to additional analysis and processing; for example, planned future projects include 3-D prestack migration. which will use the complete 3-D wavefields. Synthetic data volumes are also of potential value in pre-experiment survey design and evaluation.

The feasibility of using 3-D numerical modeling as an aid to analysis and interpretation is demonstrated. Application has been extended from previous studies. in which only synthetic data were considered. to physical model data in this study. The pseudospectral calculations are able to approximately reproduce the scale model data, and to illustrate some of the shortcomings of both numerical and physical modeling.

ACKNOWLEDGMENTS

This research was funded by CRAY Research Inc., the sponsors of the UT-Dallas Geophysical Consortium, and the NSF under grant EAR-9204610. The scale model data were acquired under the supervision of K. K. Sekharan at the University of Houston, in a project funded by BP Exploration: the assistance of Y. T. Chon and W. R. Turpening of BP Exploration was much appreciated. Computations were performed on a CRAY-YMP at the UT Center for High Performance Computing. Kuo Wu of CRAY Research Inc. assisted with implementation of efficient 3-D Fourier transforms. The manuscript was expertly typed by Anna Marie Radasinovich. Contribution No. 730 from the Program in Geosciences at The University of Texas at Dallas.

(text continues on page 133)

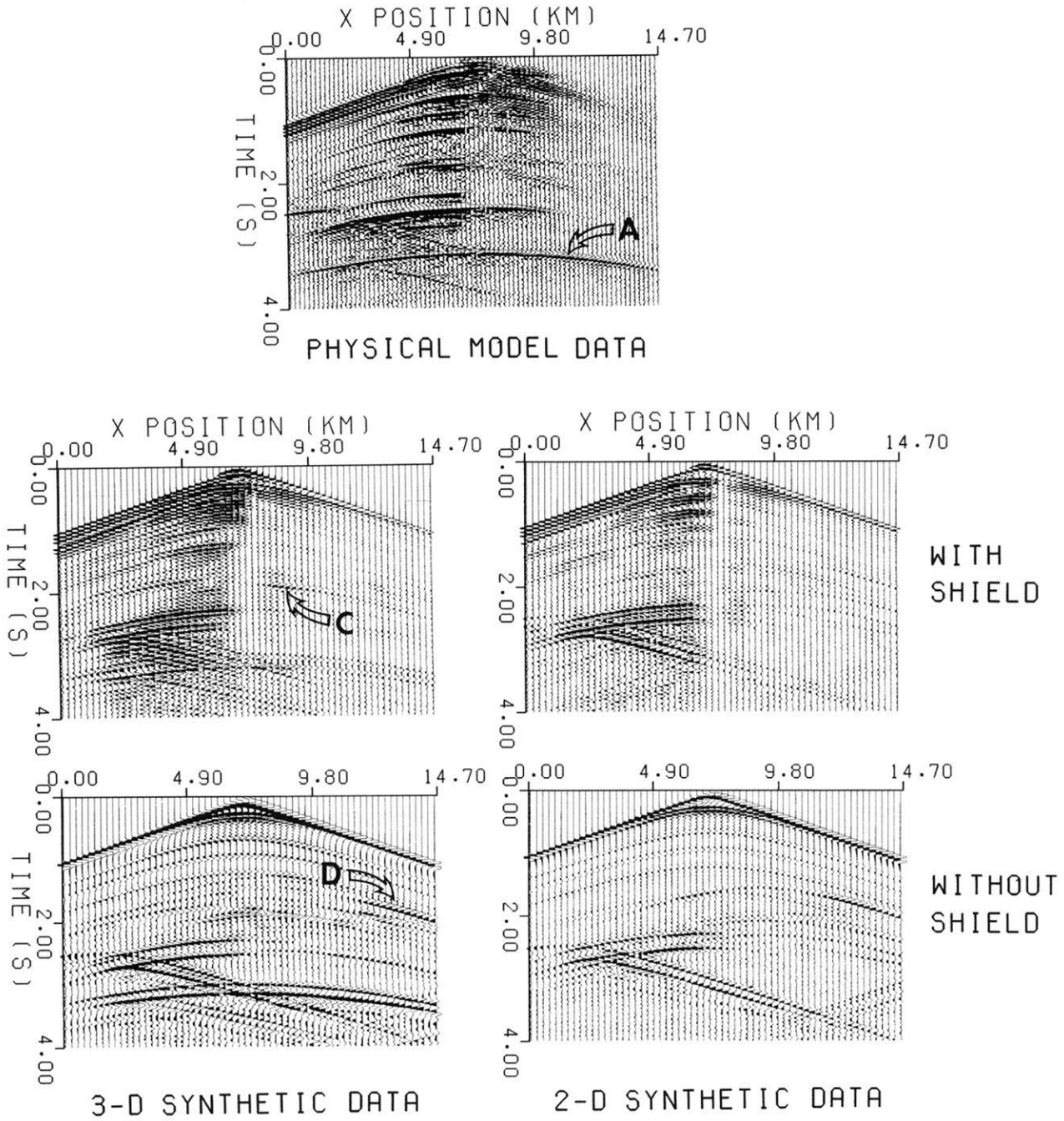

FIG. 7. Physical model (top) and synthetic (center and bottom) data for source 1 recorded on slice Y4 through the source. Reflection A is from the side of the model, C and D are from the salt. Synthetics are for both 3-D (left) and 2-D (right) modeling, and both with (center) and without (bottom) the source shield.

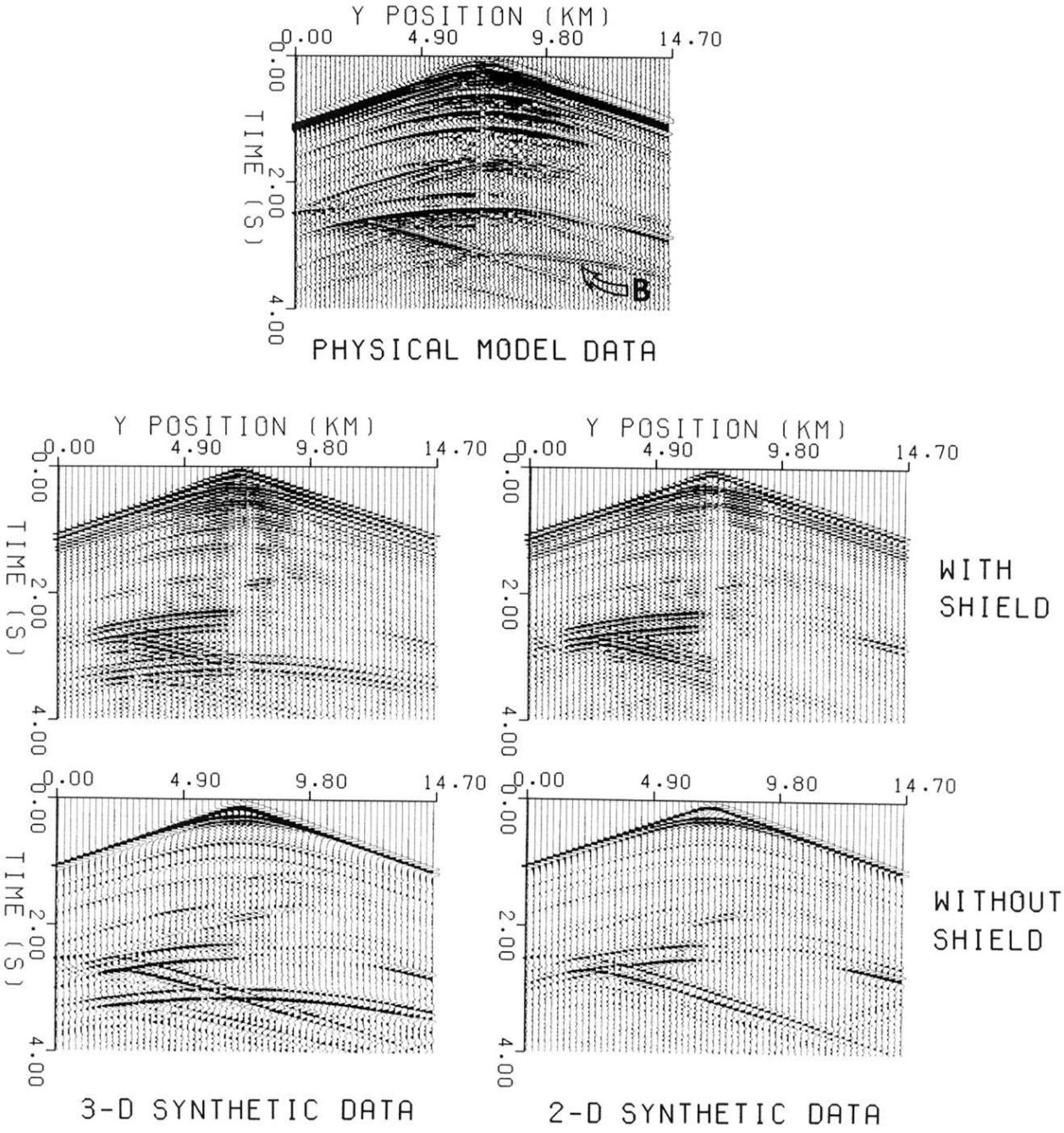

FIG. 8. Physical model (top) and synthetic (center and bottom) data for source 1 recorded on slice X4 through the source. Synthetics are for both 3-D (left) and 2-D (right) modeling, and both with (center) and without (bottom) the source shield.

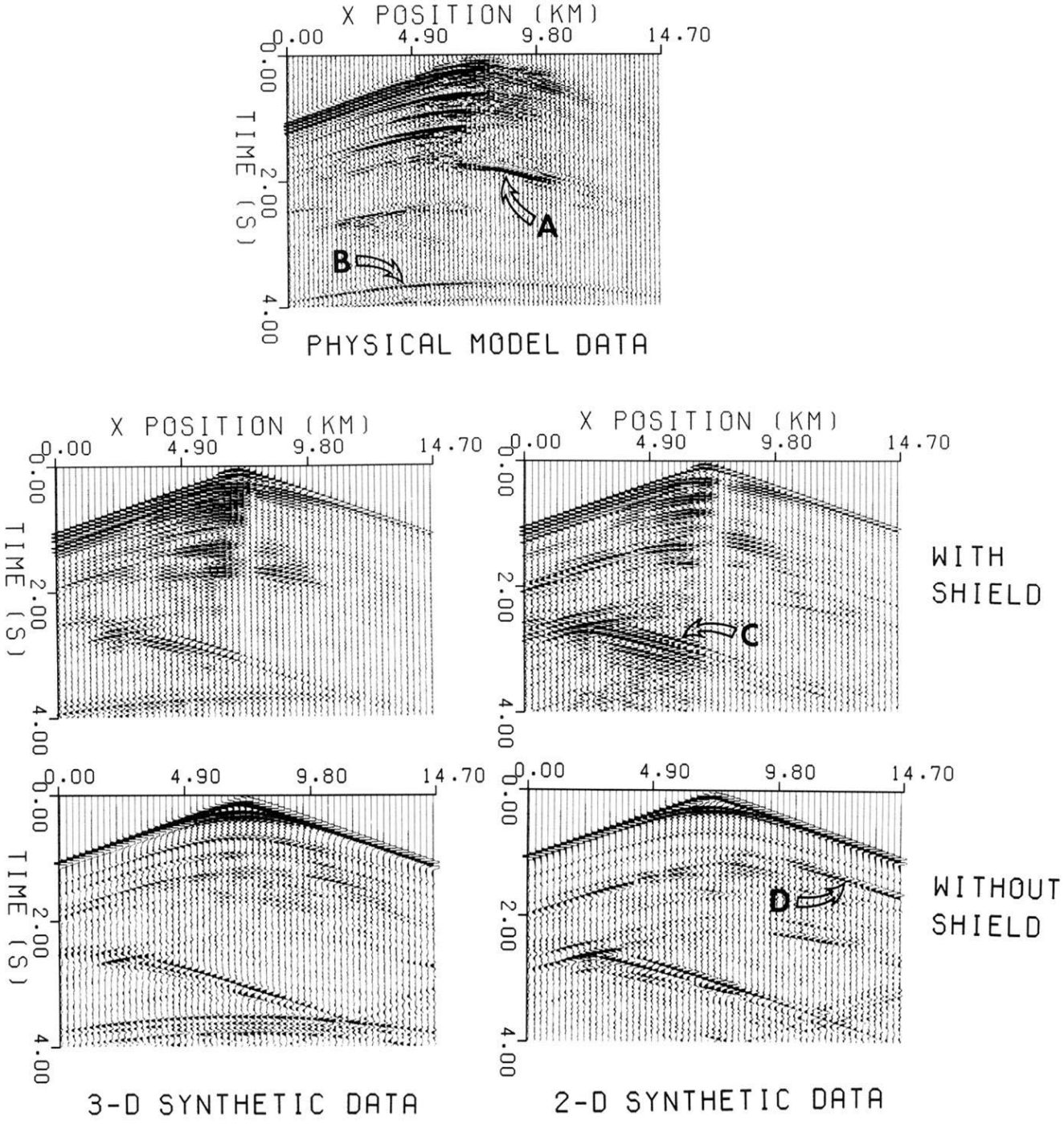

FIG. 9. Physical model (top) and synthetic (center and bottom) data for source 6 recorded on slice Y5 through the source. Synthetics are for both 3-D (left) and 2-D (right) modeling, and both with (center) and without (bottom) the source shield. Reflections A and D are from the salt.

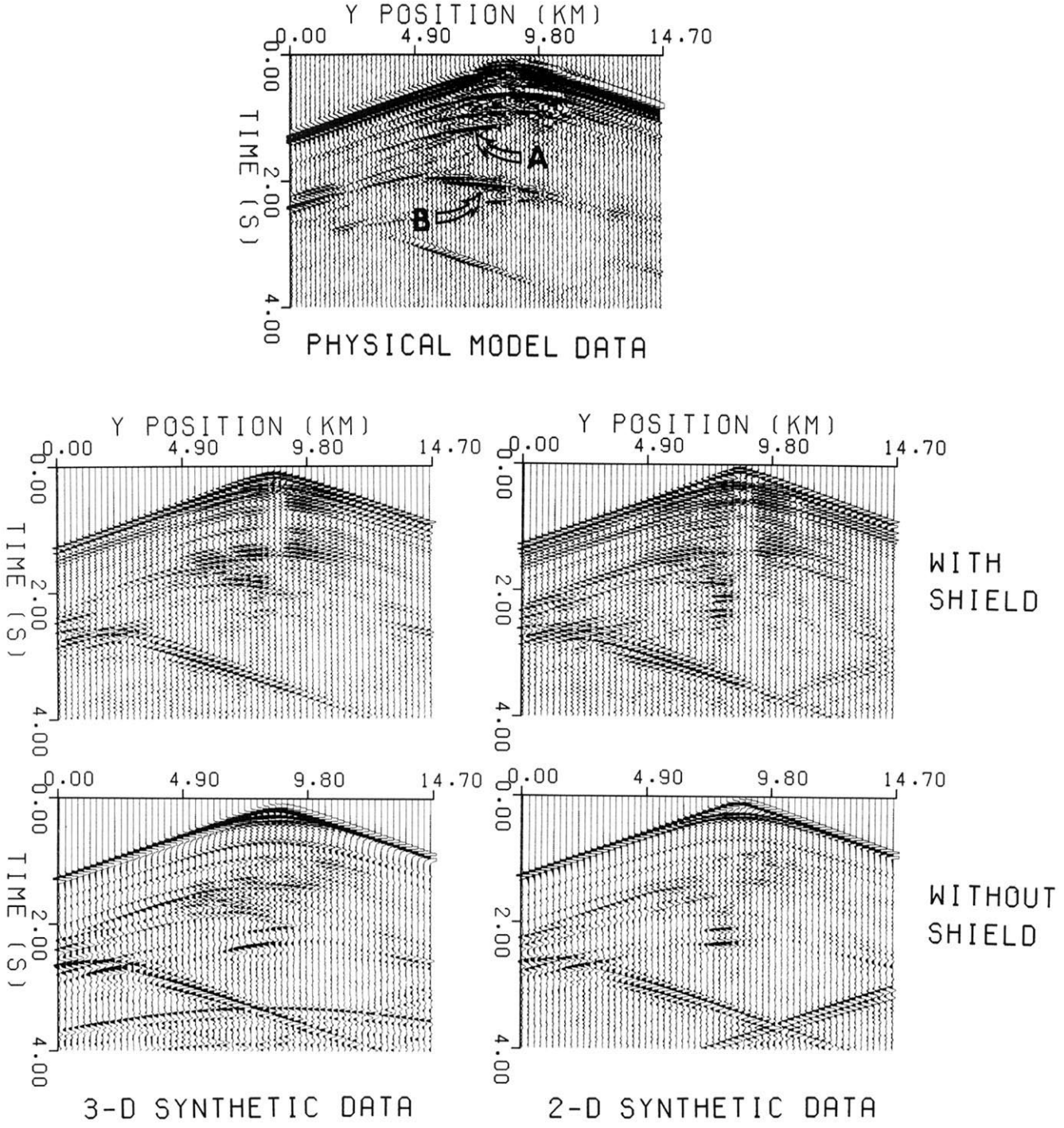

FIG. 10. Physical model (top) and synthetic (center and bottom) data for source 7 recorded on slice X6 which goes approximately through the source. Synthetics are for both 3-D (left) and 2-D (right) modeling, and both with (center) and without (bottom) the source shield. Reflections A and B are from the salt.

REFERENCES

Cerjan, C., Kosloff, D., Kosloff, R., and Reshef, M., 1985, A nonreflecting boundary condition for discrete acoustic and elastic wave equations: Geophysics, 50, 705-708.

Chang, W. F., and McMechan, G. A., 1989, Absorbing boundary conditions for 3-D acoustic and elastic finite-difference calculations: Bull. Seis. Soc. Am., 79, 211-218.

——1990, 3-D acoustic prestack reverse-time migration: Geophys. Prosp., 38, 737-755.

Chon, Y. T., and Turpening, W. R., 1990, Complex salt and subsalt imaging: A seismic physical model study in 2-D and 3-D: 60th Ann. Internat. Mtg., Soc. Expl. Geophys., Expanded Abstracts, 1569-1571.

Daudt, C. R., Braile, L. W., Nowack, R. L., and Chiang, C. S., 1989, A comparison of finite-difference and Fourier method calculations of synthetic seismograms: Bull. Seis. Soc. Am., 79, 1210-1230.

Dong, Z., and McMechan, G. A., 1991, Numerical modeling of seismic waves with a 3-D anisotropic scalar wave equation: Bull. Seis. Soc. Am., 81, 769-780.

—— 1993, 3-D prestack migration in anisotropic media: Geophysics, 58, 79-90.

Ebrom, D, A., Tatham, R. H., Sekharan, K. K., McDonald, J. A., and Gardner, G. H. F., 1990, Hyperbolic traveltime analysis of first arrivals in an azimuthally anisotropic medium: A physical modeling study: Geophysics, 55, 185-191.

Fornberg, B., 1987, The pseudospectral method: Comparisons with finite-differences for the elastic wave equation: Geophysics, 52, 483-501.

Gazdag, J., 1973, Numerical convective schemes based on accurate computation of space derivatives: J. Comp. Phys., 13, 1175-1183.

Gregory, A. R., 1977, Aspects of rock physics from laboratory and log data that are important to seismic interpretation: Am. Assoc. Petrol. Geol. Memoir, 26, 15-46.

Holberg, O., 1987, Computational aspects of the choice of operation and sampling interval of numerical differentiation in large-scale simulation of wave phenomena: Geophys. Prosp., 35, 629-655.

Kosloff, D., and Baysal, E., 1982, Forward modeling by a Fourier method: Geophysics, 47, 1402-1412.

Kreiss, H. O., and Oliger, J., 1972, Comparison of accurate methods for the integration of hyperbolic equations: Tellus, 24, 199-255.

Ladzekpo, D. H., Sekharan, K. K., and Gardner, G. H. F., 1988, Physical modeling for hydrocarbon exploration: 58th Ann. Internat. Mtg., Soc. Expl. Geophys., Expanded Abstracts, 586-588.

Lu, L., and Herbert, V., 1989, Depth imaging of physical model data: 59th Ann. Internat. Mtg., Soc. Expl. Geophys., Expanded Abstracts, 1187-1189.

Mora, P., 1989, Modeling anisotropic seismic waves in 3-D: 59th Ann. Internat. Mtg., Soc. Expl. Geophys., Expanded Abstracts, 1039-1043.

Mufti, I. R., 1989, Numerical experiments with a salt dome: Geophysics, 54, 1042-1045.

——1990, Large-scale three-dimensional seismic models and their' interpretive significance: Geophysics, 55, 1166-1182.

Mufti, I. R., and Fou, J. T., 1989, Application of three-dimensional finite-difference seismic modeling in oil field exploitation and simulation: Internat. J. Imag. Sys. Tech., 1, 28-32.

Orzag, S. A., 1981, Spectral methods for problems in complex geometries, J. Comp. Phys., 37, 70-92.

Reshef, M., 1991, Prestack depth imaging of three-dimensional shot gathers: Geophysics, 56, 1158-1163.

Reshef, M., Kosloff, D., Edwards, M., and Hsiung, C., 1988a, Three-dimensional acoustic modeling by the Fourier method: Geophysics, 53, 1175-1183.

——1988b, Three-dimensional elastic modeling by the Fourier method: Geophysics, 53, 1184-1193.

Yoon, K. H., and McMechan, G. A., 1991, 3-D finite-difference modeling of elastic waves in borehole environments: Geophysics, 57, 793-804.